analytical chemistry

pubs.acs.org/ac Letter

Multiscale Evolution of Bulk Heterojunction Solar Cell Active Layers under Thermal Stress

Fei Zhao, Seth L. Filbrun, Tengxiang Huang, Bin Dong,* and Ning Fang*

Cite This: https://dx.doi.org/10.1021/acs.analchem.0c04461 Read Online

ACCESS | Metrics & More | Article Recommendations | Supporting Information

ABSTRACT: A multimodality spectromicroscopy imaging system has been developed to offer the essential capability of in situ characterization of functional materials at multiple length scales during the morphology evolution and phase development under external stimuli. The photoactive layer of bulk heterojunction solar cell, whose performance is strongly correlated to the structural features over a wide range of length scales, was characterized under thermal stress. Three stages of thermotropic evolution were monitored continuously by the spectromicroscopy imaging system to reveal the critical information from the molecular level to meso- and microscale. The optimized thermal annealing temperature window and preferred temperature dropping operation were identified to promote the performance of the photoactive layer.

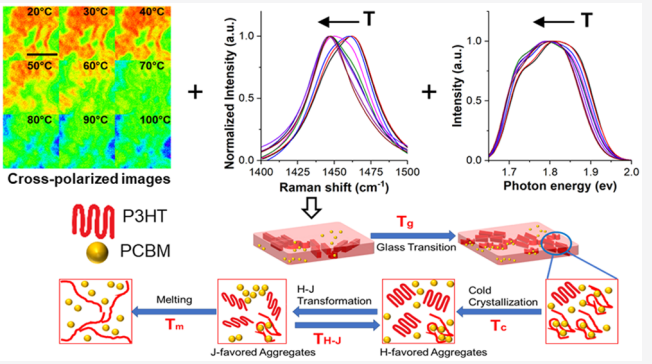

Structural features of functional materials across a wide range of length scales are essential to their performance. As a prominent example, structures of organic semiconducting materials, ranging from the $\pi-\pi$ stackings at the molecular and nanoscale level to charge transport pathways at the meso- (typically defined as 100−1000 nm), micro-, and macroscopic scales, can profoundly affect the optoelectronic properties and their consequent performance in organic optoelectronic devices, including organic thin-film field-effect transistors (FETs), organic light-emitting diodes (LEDs), and organic photovoltaics cells.[1−4] However, it is challenging to obtain information spanning many orders of magnitude in length scale correlatively in situ using conventional characterization methods,[4−7] which restrains our understanding of the inherent hierarchical structures of organic semiconductors and their structure−property relationship.

Optical microscopy imaging is inherently suited for studying mesoscale and microscale structures and dynamics for its matching resolution range of tens to hundreds of nanometers. It is much less invasive compared to other characterization methods such as electron microscopy, where high-energy electron beams could damage the sample, especially fragile crystalline structures in organic films.[5] On the other hand, spectroscopic techniques (Raman, photoluminescence, etc.) are usually required as companion tools to study molecular conformations and provide an important insight into the fundamental structure−property relationships.[8−10] In the present study, we designed and built a multimodality spectromicroscopy imaging system (Figures 1a and S1) to combine far-field cross-polarized light microscopy with confocal Raman and photoluminescence spectroscopy for the in situ characterization of samples prepared on reflective surfaces, such as silicon wafers and metal-coated substrates, under external stimuli.

Photoactive layers in bulk heterojunction (BHJ) solar cells, composed of a mixture of polymer semiconductors as electron donor and hole-conducting material and acceptor material, self-assemble into polydisperse irregularly shaped domains.[11] Utilizing a home-built thermal annealing microscope stage (Figure S1), the spectromicroscopy system has been employed for an in situ multiscale correlative study of the thermotropic evolution of poly(3-hexylthiophene) (P3HT) and [6,6]-phenyl C61 butyric acid methyl ester (PCBM) blend thin films of 1:1 stoichiometry, a common example of photoactive layers in BHJ solar cells. As reported previously, there are crystalline P3HT, PCBM crystals, and a mixture of amorphous P3HT and PCBM in the 1:1 P3HT/PCBM blend thin film.[12] Postdeposition treatment, such as thermal annealing,[13−15] is commonly used to improve the performance of the thin-film electronics.[16,17] Many studies of the photovoltaic blends have been conducted under high temperatures.[18−23] The high temperature leads to an increased molecular mobility, which results in the spatial rearrangement of the polymer chains and the diffusion of PCBM molecules.[21] By using TEM, it has been reported that

Received: October 22, 2020
Accepted: December 15, 2020

https://dx.doi.org/10.1021/acs.analchem.0c04461
Anal. Chem. XXXX, XXX, XXX−XXX

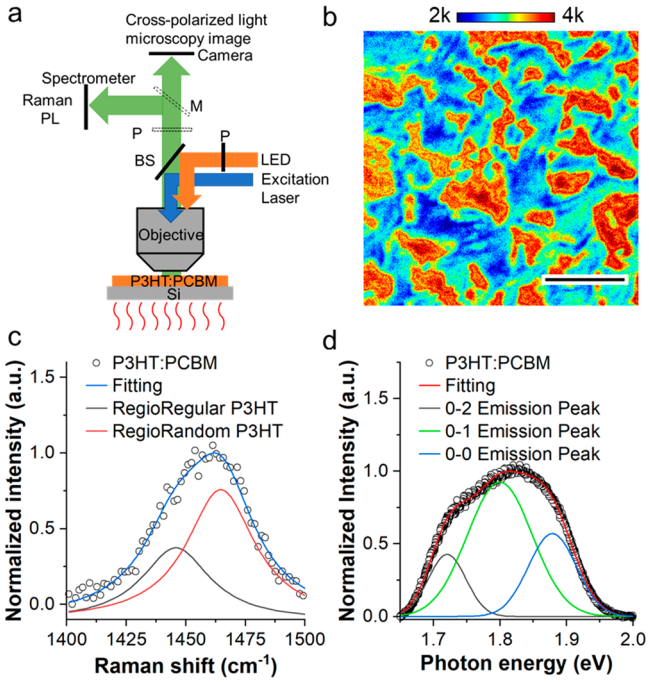

Figure 1. Characterization of the 1:1 P3HT/PCBM blend thin film at room temperature. (a) Schematic of the spectromicroscopy imaging system. P: linear polarizer; BS: beam splitter; M: mirror. Components in the dashed outline are removable for different modules. (b) Cross-polarized microscopy image of the film on the Si substrate. The scale bar is 5 μm. (c) Raman and (d) PL spectra of the same sample in (b). The Raman and PL spectra were averaged from 10 measurements in the sample area.

crystalline P3HT is formed after annealing the blend thin film at 80 °C for 5 min, which leads to an increase of the hole mobility.[17]

During the thermotropic evolution under the protection of nitrogen, temperature was first increased at a rate of 10 °C/min from room temperature (~20 °C) to 100 °C and then dropped either at a rate of 5 °C/min or uncontrollably back down to room temperature. More experimental details are provided in Supporting Information S2. Three spectromicroscopy measurements including cross-polarized light microscopy images, Raman spectra, and photoluminescence (PL) spectra were taken on the same sample region at each temperature setting. Structural features ranging from the molecular level to mesoscale, microscale in the 1:1 P3HT/PCBM thin films, and their corresponding dynamic changes in thermal annealing were then uncovered on the basis of these spectromicroscopy measurements.

First, cross-polarized light microscopy was used to characterize the mesoscale and microscale features in the as-cast blend thin film of 1:1 P3HT/PCBM. The microscopy images captured under cross-polarized light display domains of different contrasts (Figures 1b and S3a), indicating that these mesoscale domains are anisotropic with dominant orientations (Supporting Information S3.1). These orientational domains are not pure single crystalline domains, and they are assemblies of many crystalline domains at the microscale. The bright and dark contrast regions give rise to a bimodal distribution of pixel intensity (Figure S3c).[24] The domain orientation features are not observed in the bright field microscopy images under unpolarized light illumination (Figure S3b,d), suggesting the polarization-averaged images cannot resolve the orientational heterogeneity in the as-cast 1:1 P3HT/PCBM thin films. The cross-polarized light microscopy images of regioregular and regiorandom P3HT are shown in Figure S4. There are domain patterns with different contrasts in pure regioregular P3HT resulting from its rigid structures. In contrast, there are no domain patterns in pure regiorandom P3HT. Characterization of the mesoscale orientational domains in the thin films is essential for understanding the optoelectronic properties, such as charge transport[25,26] and absorption of unpolarized light.[27]

Second, on the molecular level, Raman spectroscopy was used to characterize the degree of crystallinity in the photoactive blend thin films relative to a pristine regioregular P3HT film. Since the Raman and PL signals from PCBM overlap with that from P3HT and are significantly lower than those from P3HT,[28−30] we therefore attribute the Raman and PL signals to P3HT in the photoactive blend thin films. The C═C Raman peaks from P3HT in a blend thin film (Figure 1c) can be deconvoluted into regioregular (RR, ordered) and regiorandom (RRa, disordered) peaks (Figure S5). The relative degree of crystallinity of the P3HT blending with PCBM is quantified as the fraction of the ordered P3HT phase.[31] Details of Raman spectra analysis are provided in Supporting Information S3.2.

Third, photoluminescence (PL) spectroscopy was utilized to distinguish the two types of aggregates, that is H-favored and J-favored (Figure 2e),[32−35] formed by emissive polymeric semiconductors. The type of aggregate depends on the relative alignment of the transition dipoles of adjacent molecules in stackings.[36−38] The PL spectra can be deconvoluted into 0−0, 0−1, and 0−2 emission peaks (Figure 1d). The 0−0 emission peak is substantially attenuated for H-favored aggregates, while enhanced for J-favored aggregates.[32,34,35,38] Therefore, the ratio of 0−0 to 0−1 emission peaks ($I_{PL}^{0-0}/I_{PL}^{0-1}$) can be used to identify different types of aggregates in the blend thin film.[35] Details of PL spectra analysis are provided in Supporting Information S3.3.

The in situ correlative study using these three techniques offered a more complete understanding of the thermotropic evolution. As shown in Figure 2, transformations started after the sample was heated to above the glass transition temperature (T_g)[39] of ~30 °C, when amorphous P3HT on the molecular level began to obtain flexibility. This was then followed by cold crystallization (T_{cc}) and the transformation from H- to J-favored aggregates ($T_{H\text{-}J}$) at higher temperatures. The degree of crystallinity−temperature correlation (Figures 2d and S7) was fitted with a sigmoid function (Supporting Information S3.2). T_{cc} could then be identified to be 49 °C from the first derivative curve of the sigmoid fitting function (Figure S8). Moreover, two other critical temperatures (T_{cc}^{min} and T_{cc}^{max}) that corresponded to the start and end of the cold crystallization process[40] were calculated (Supporting Information S3.4) to be 30 and 84 °C, respectively. The thermotropic alignment and merging of the mesoscale orientational domains were first observed at the domain boundaries (Figures 2a, S9, and S10), where a higher amorphous polymer composition existed. The thermotropic alignment of the orientational domains described by the merging of intensity distribution peaks (Figure S11) agrees with the evolution process shown in Figures 2a and S9. However, the blend thin film split into the domains of various dominant orientations again at 80 °C (Figure 2b). Moreover, the change of the peak ratio of 0−0 to 0−1 emission peaks ($I_{PL}^{0-0}/I_{PL}^{0-1}$) with increasing temperature

https://dx.doi.org/10.1021/acs.analchem.0c04461
Anal. Chem. XXXX, XXX, XXX−XXX

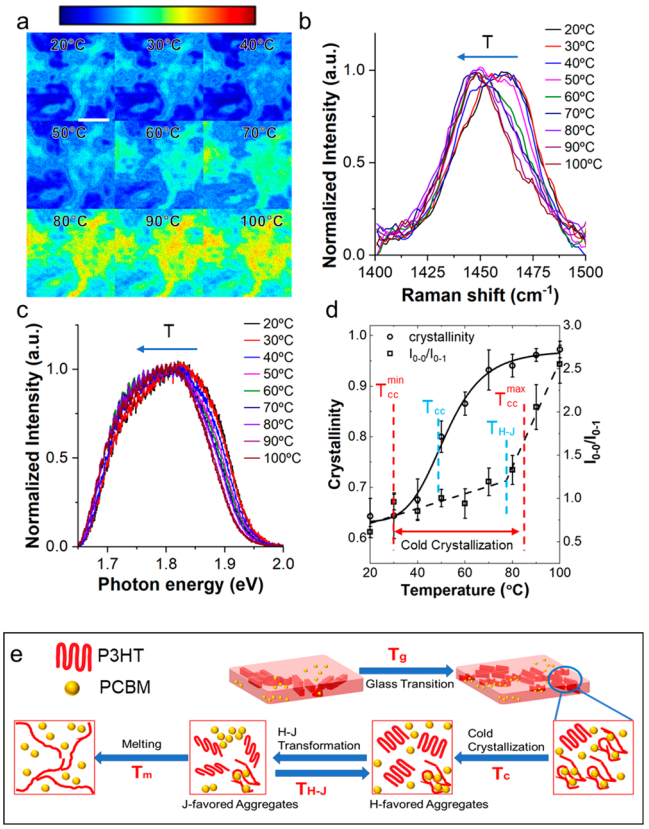

Figure 2. Thermotropic evolution of the 1:1 P3HT/PCBM blend thin film from 20 to 100 °C. (a) Cross-polarized microscopy images of the same sample region at different temperatures. The scale bar is 2.5 μm. (b) Raman and (c) PL spectra at different temperatures. These spectra were averaged from 10 measurements at different regions of the sample. (d) The evolution of the degree of crystallinity and I_{0-0}/I_{0-1} calculated from Raman and PL spectra, respectively. The solid line is the sigmoid fitting of the degree of crystallinity vs temperature. The dashed line is the two piecewise linear fitting of I_{0-0}/I_{0-1} vs temperature. The error bars show the standard deviations of 10 measurements. (e) The schematic diagram of the thermotropic evolution process.

(Figures 2c, d and S12) was fitted with two piecewise linear functions (Figure 2d), and the transformation temperature ($T_{H\text{-}J}$) from H- to J-favored aggregates[41] was identified to be ~77 °C from the intersection of the two linear functions. Finally, the melting process would happen at ~150 °C;[42] however, it was beyond the technical limit of our spectromicroscopy system. On the basis of these results, the entire thermotropic evolution is depicted in Figure 2e.

These in situ multiscale measurements unravel the thermotropic evolution process and provide direct experimental evidence for the optimization of the photoactive layers in BHJ solar cells. There are two optimization factors at the mesoscale and molecular level, respectively. On the mesoscale, blend thin films with high orientational order are favored because domain boundaries affect the charge carrier transportation adversely[43] and more uniform orientation results in higher charge mobility.[24] Therefore, on the basis of the characterization from mesoscale, a thermal annealing temperature above ~70 °C is necessary (Figure S11). On the molecular level, studies showed that J-favored aggregates offer higher exciton mobilities, larger exciton diffusion lengths,[36,37] and an order of magnitude higher power conversion efficiency than H-favored aggregates.[38] Hence, J-favored aggregates are preferred in photoactive layers in BHJ solar cells, and a thermal annealing temperature above the transition temperature $T_{H\text{-}J}$ (~77 °C) but lower than the cold crystallization of PCBM (~130 °C)[42] is necessary (Figure 2d).

After heating the thin film sample to 100 °C, we cooled the sample down to the room temperature while taking similar measurements using the spectromicroscopy system. The results are shown in Figure 3. Two temperature dropping

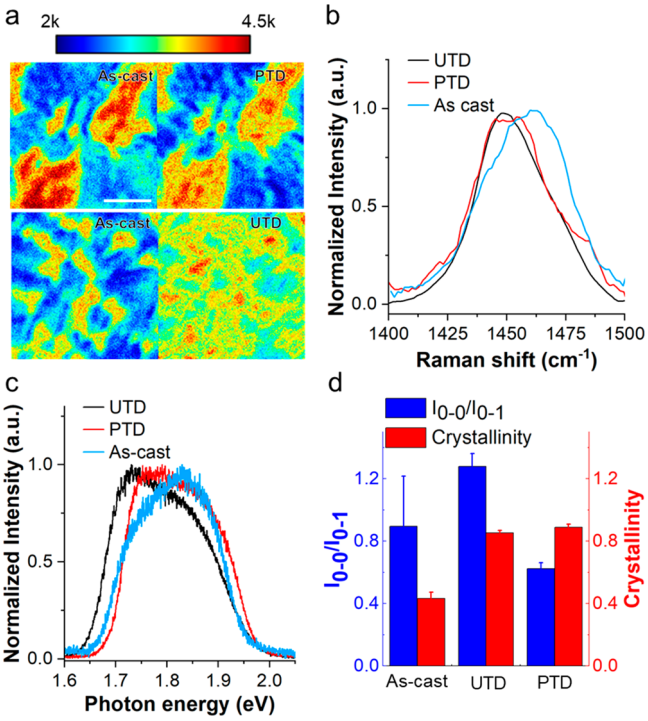

Figure 3. Comparison of the 1:1 P3HT/PCBM blend thin film processed by programmed and uncontrolled temperature dropping. (a) Cross-polarized microscopy images of the same sample regions before and after programmed temperature dropping (PTD) (top two images) or uncontrolled temperature dropping (UTD) (bottom two images). (b) Raman spectra, (c) PL spectra, and (d) I_{0-0}/I_{0-1} and the degree of crystallinity of the as-cast, PTD, and UTD samples. The error bars show the standard deviations of 10 measurements.

methods were applied: programmed or uncontrolled temperature dropping, namely, PTD and UTD, respectively. Mesoscale structures were restored, and the orientational order in each domain was enhanced after programmed temperature dropping (Figures 3a, top and S13a–d). In contrast, after uncontrolled temperature dropping, the patterns of the mesoscale orientational domains were lost, and a blend thin film with high orientational order was obtained (Figures 3a, bottom and S13e–h). For the molecular level structural information, there was no significant difference in the Raman spectra (Figure 3b) or the degree of crystallinity (Figure 3d, red) of the annealed blend thin film processed by two temperature dropping procedures. However, the photoluminescence spectra (Figure 3c) were different. The $I_{PL}^{0-0}/I_{PL}^{0-1}$ (Figure 3d, blue) of the blend thin film processed by uncontrolled temperature dropping was significantly higher than that processed by programmed temperature dropping (Student's t test $p < 0.05$), which implies different types of polymeric aggregates obtained by the two temperature

https://dx.doi.org/10.1021/acs.analchem.0c04461
Anal. Chem. XXXX, XXX, XXX−XXX

dropping procedures. As shown in Figure 2d, there are two stages of the $I_{PL}^{0-0}/I_{PL}^{0-1}$−temperature curve during the thermotropic evolution. When temperature dropped quickly (uncontrollably), the J-favored aggregates were maintained; however, during the programmed temperature dropping, the polymeric aggregates changed gradually and were able to transform from J-favored back to H-favored. When information on the mesoscale and molecular levels are combined, the results explain why the fast temperature dropping process is preferred as post-treatment for photoactive layers.

In summary, the in situ multiscale spectromicroscopy system successfully characterized the photoactive layers of the BHJ solar cell in a wide range of length scales under thermal stress. The correlative evolution of mesoscale structures and molecular conformations was revealed experimentally. The optimized thermal annealing temperature window and the preferred temperature dropping operation method in thermal annealing were therefore identified on the basis of the three phase transition stages during the thermotropic evolution. The molecular packing can be effectively tuned by temperature and post-treatment operation. Through this study, we demonstrate the essential capability of in situ characterization at multiple length scales to monitor the morphology evolution and phase development and identify critical changes of complex functional materials under external stimuli.

■ ASSOCIATED CONTENT

Supporting Information

The Supporting Information is available free of charge at https://pubs.acs.org/doi/10.1021/acs.analchem.0c04461.

Experimental details, cross-polarized light microscopy images analysis, Raman and photoluminescence spectra analyses, calculations, diagram and picture of the instrument, laser spot and Gaussian fitting, microscopy images and intensity distributions, Raman spectra, evolution of the degree of crystallinity, mesoscale and thermotropic evolution, and change of overlap (PDF)

■ AUTHOR INFORMATION

Corresponding Authors

Ning Fang − *Department of Chemistry, Georgia State University, Atlanta, Georgia 30303, United States;* orcid.org/0000-0003-4710-0984; Email: nfang@gsu.edu

Bin Dong − *Department of Chemistry, Georgia State University, Atlanta, Georgia 30303, United States;* Email: bdong@gsu.edu

Authors

Fei Zhao − *Department of Chemistry, Georgia State University, Atlanta, Georgia 30303, United States*

Seth L. Filbrun − *Department of Chemistry, Georgia State University, Atlanta, Georgia 30303, United States*

Tengxiang Huang − *Department of Chemistry, Georgia State University, Atlanta, Georgia 30303, United States;* orcid.org/0000-0002-4428-3175

Complete contact information is available at: https://pubs.acs.org/10.1021/acs.analchem.0c04461

Notes

The authors declare no competing financial interest.

■ ACKNOWLEDGMENTS

This work was supported by the fund from Georgia State University.

■ REFERENCES

(1) Treat, N. D.; Westacott, P.; Stingelin, N. *Annu. Rev. Mater. Res.* **2015**, *45* (1), 459.

(2) Takacs, C. J.; Treat, N. D.; Krämer, S.; Chen, Z.; Facchetti, A.; Chabinyc, M. L.; Heeger, A. J. *Nano Lett.* **2013**, *13* (6), 2522.

(3) Wang, H.; Xu, Y.; Yu, X.; Xing, R.; Liu, J.; Han, Y. *Polymers* **2013**, *5* (4), 1272.

(4) Treat, N. D.; Chabinyc, M. L. *Annu. Rev. Phys. Chem.* **2014**, *65* (1), 59.

(5) Panova, O.; Ophus, C.; Takacs, C. J.; Bustillo, K. C.; Balhorn, L.; Salleo, A.; Balsara, N.; Minor, A. M. *Nat. Mater.* **2019**, *18*, 860.

(6) Salleo, A.; Chen, T. W.; Völkel, A. R.; Wu, Y.; Liu, P.; Ong, B. S.; Street, R. A. *Phys. Rev. B: Condens. Matter Mater. Phys.* **2004**, *70* (11), 115311.

(7) Herzing, A. A.; Richter, L. J.; Anderson, I. M. *J. Phys. Chem. C* **2010**, *114* (41), 17501.

(8) Honea, E. C.; Ogura, A.; Murray, C. A.; Raghavachari, K.; Sprenger, W. O.; Jarrold, M. F.; Brown, W. L. *Nature* **1993**, *366* (6450), 42.

(9) Donley, C. L.; Zaumseil, J.; Andreasen, J. W.; Nielsen, M. M.; Sirringhaus, H.; Friend, R. H.; Kim, J.-S. *J. Am. Chem. Soc.* **2005**, *127* (37), 12890.

(10) Schmidtke, J. P.; Kim, J.-S.; Gierschner, J.; Silva, C.; Friend, R. H. *Phys. Rev. Lett.* **2007**, *99* (16), 167401.

(11) Sharenko, A.; Kuik, M.; Toney, M. F.; Nguyen, T.-Q. *Adv. Funct. Mater.* **2014**, *24* (23), 3543.

(12) Yin, W.; Dadmun, M. *ACS Nano* **2011**, *5* (6), 4756.

(13) Treat, N. D.; Shuttle, C. G.; Toney, M. F.; Hawker, C. J.; Chabinyc, M. L. *J. Mater. Chem.* **2011**, *21* (39), 15224.

(14) Jimison, L. H.; Salleo, A.; Chabinyc, M. L.; Bernstein, D. P.; Toney, M. F. *Phys. Rev. B: Condens. Matter Mater. Phys.* **2008**, *78* (12), 125319.

(15) Luzio, A.; Nübling, F.; Martin, J.; Fazzi, D.; Selter, P.; Gann, E.; McNeill, C. R.; Brinkmann, M.; Hansen, M. R.; Stingelin, N.; Sommer, M.; Caironi, M. *Nat. Commun.* **2019**, *10* (1), 3365.

(16) Hopkinson, P. E.; Staniec, P. A.; Pearson, A. J.; Dunbar, A. D. F.; Wang, T.; Ryan, A. J.; Jones, R. A. L.; Lidzey, D. G.; Donald, A. M. *Macromolecules* **2011**, *44* (8), 2908.

(17) Savenije, T. J.; Kroeze, J. E.; Yang, X.; Loos, J. *Adv. Funct. Mater.* **2005**, *15* (8), 1260.

(18) Treat, N. D.; Mates, T. E.; Hawker, C. J.; Kramer, E. J.; Chabinyc, M. L. *Macromolecules* **2013**, *46* (3), 1002.

(19) Labram, J. G.; Fabini, D. H.; Perry, E. E.; Lehner, A. J.; Wang, H.; Glaudell, A. M.; Wu, G.; Evans, H.; Buck, D.; Cotta, R.; Echegoyen, L.; Wudl, F.; Seshadri, R.; Chabinyc, M. L. *J. Phys. Chem. Lett.* **2015**, *6* (18), 3565.

(20) Lindqvist, C.; Bergqvist, J.; Feng, C.-C.; Gustafsson, S.; Bäcke, O.; Treat, N. D.; Bounioux, C.; Henriksson, P.; Kroon, R.; Wang, E.; Sanz-Velasco, A.; Kristiansen, P. M.; Stingelin, N.; Olsson, E.; Inganäs, O.; Andersson, M. R.; Müller, C. *Adv. Energy Mater.* **2014**, *4* (9), 1301437.

(21) Campoy-Quiles, M.; Ferenczi, T.; Agostinelli, T.; Etchegoin, P. G.; Kim, Y.; Anthopoulos, T. D.; Stavrinou, P. N.; Bradley, D. D. C.; Nelson, J. *Nat. Mater.* **2008**, *7* (2), 158.

(22) Guo, T.-F.; Wen, T.-C.; L'Vovich Pakhomov, G.; Chin, X.-G.; Liou, S.-H.; Yeh, P.-H.; Yang, C.-H. *Thin Solid Films* **2008**, *516* (10), 3138.

(23) Yang, X.; Loos, J.; Veenstra, S. C.; Verhees, W. J. H.; Wienk, M. M.; Kroon, J. M.; Michels, M. A. J.; Janssen, R. A. J. *Nano Lett.* **2005**, *5* (4), 579.

(24) Pingel, P.; Zen, A.; Abellón, R. D.; Grozema, F. C.; Siebbeles, L. D. A.; Neher, D. *Adv. Funct. Mater.* **2010**, *20* (14), 2286.

(25) Redecker, M.; Bradley, D. D. C.; Inbasekaran, M.; Woo, E. P. *Appl. Phys. Lett.* **1999**, *74* (10), 1400.

https://dx.doi.org/10.1021/acs.analchem.0c04461
Anal. Chem. XXXX, XXX, XXX−XXX

(26) Sirringhaus, H.; Wilson, R. J.; Friend, R. H.; Inbasekaran, M.; Wu, W.; Woo, E. P.; Grell, M.; Bradley, D. D. C. *Appl. Phys. Lett.* **2000**, *77* (3), 406.
(27) Takacs, C. J.; Collins, S. D.; Love, J. A.; Mikhailovsky, A. A.; Wynands, D.; Bazan, G. C.; Nguyen, T.-Q.; Heeger, A. J. *ACS Nano* **2014**, *8* (8), 8141.
(28) Gao, Y.; Grey, J. K. *J. Am. Chem. Soc.* **2009**, *131* (28), 9654.
(29) Motaung, D. E.; Malgas, G. F.; Arendse, C. J.; Mavundla, S. E.; Knoesen, D. *Mater. Chem. Phys.* **2009**, *116* (1), 279.
(30) Malgas, G. F.; Arendse, C. J.; Mavundla, S.; Cummings, F. R. *J. Mater. Sci.* **2008**, *43* (16), 5599.
(31) Tsoi, W. C.; James, D. T.; Kim, J. S.; Nicholson, P. G.; Murphy, C. E.; Bradley, D. D. C.; Nelson, J.; Kim, J.-S. *J. Am. Chem. Soc.* **2011**, *133* (25), 9834.
(32) Spano, F. C. *J. Chem. Phys.* **2005**, *122* (23), 234701.
(33) Spano, F. C. *Acc. Chem. Res.* **2010**, *43* (3), 429.
(34) Spano, F. C.; Yamagata, H. *J. Phys. Chem. B* **2011**, *115* (18), 5133.
(35) Spano, F. C.; Silva, C. *Annu. Rev. Phys. Chem.* **2014**, *65* (1), 477.
(36) Siebbeles, L. D. A.; Huijser, A.; Savenije, T. J. *J. Mater. Chem.* **2009**, *19* (34), 6067.
(37) Tennakone, K.; Pitigala, P. K. D. D. P.; Perera, A. G. U. *RSC Adv.* **2013**, *3* (8), 2770.
(38) Más-Montoya, M.; Janssen, R. A. J. *Adv. Funct. Mater.* **2017**, *27* (16), 1605779.
(39) Demir, F.; Van den Brande, N.; Van Mele, B.; Bertho, S.; Vanderzande, D.; Manca, J.; Van Assche, G. *J. Therm. Anal. Calorim.* **2011**, *105* (3), 845.
(40) Mannanov, A. A.; Bruevich, V. V.; Feldman, E. V.; Trukhanov, V. A.; Pshenichnikov, M. S.; Paraschuk, D. Y. *J. Phys. Chem. C* **2018**, *122* (34), 19289.
(41) Hestand, N. J.; Spano, F. C. *J. Chem. Phys.* **2015**, *143* (24), 244707.
(42) Hajduk, B.; Bednarski, H.; Jarząbek, B.; Janeczek, H.; Nitschke, P. *Beilstein J. Nanotechnol.* **2018**, *9*, 1108.
(43) Banach, M. J.; Friend, R. H.; Sirringhaus, H. *Macromolecules* **2003**, *36* (8), 2838.

https://dx.doi.org/10.1021/acs.analchem.0c04461
Anal. Chem. XXXX, XXX, XXX−XXX